JOURNAL OF THE MECHANICAL BEHAVIOR OF BIOMEDICAL MATERIALS 64 (2016) 173–186

Available online at www.sciencedirect.com

ScienceDirect

www.elsevier.com/locate/jmbbm

Research Paper

Fracture characteristics of PEEK at various stress triaxialities

Fei Chen[a], *Shakir Gatea*[a], *Hengan Ou*[a,*], *Bin Lu*[b,c], *Hui Long*[c]

[a]*Department of Mechanical, Materials and Manufacturing Engineering, University of Nottingham, Nottingham NG7 2RD, UK*
[b]*Institute of Forming Technology and Equipment, Shanghai Jiao Tong University, 1954 Huashan Road, Shanghai 200030, PR China*
[c]*Department of Mechanical Engineering, University of Sheffield, Sheffield S1 3JD, UK*

ARTICLE INFO

Article history:
Received 12 June 2016
Received in revised form
16 July 2016
Accepted 21 July 2016
Available online 30 July 2016

Keywords:
PEEK
Stress triaxiality
Fracture
Finite element analysis

ABSTRACT

Polyether-ether-ketone (PEEK) is an alternative to metal alloys in orthopaedic applications. It gives significant advantages including excellent mechanical properties and non-toxicity. In this work, a set of specimens with different notched radii were selected to examine the effect of triaxial state of stress on the fracture behavior of PEEK. Fractographic analysis via scanning electron microscopy (SEM) and energy-dispersive X-ray spectroscopy (EDX) further elucidated the fracture micromechanisms. Distinct fracture patterns were identified under different stress triaxialities. In addition, the microstructural inclusion properties in PEEK specimen such as inclusion size and chemical composition were analysed and determined. Finite element simulations were carried out to evaluate the correlation of observed fracture characteristics with different stress triaxialities.

1. Introduction

Implants engineering has emerged as a scientific field distinct from the evolution of medical sciences and tissue engineering. Implants materials commonly used in clinic surgeries mainly include metals, ceramics, polymers and its composites. In the past decades, metallic materials, such as titanium (Ti) alloy (Diefenbeck et al., 2011), stainless steel (Agarwal et al., 2015), and shape memory alloy (NiTi) (Poon et al., 2005) have been widely used in implant engineering. Principally, metallic materials have favourable mechanical strength, excellent friction resistance and non-toxic properties. However, there are also limitations of metallic systems which hinder their universal acceptance in medical applications. Firstly, the strength and elastic modulus of metal and its alloys are much higher than those of human bone tissues. For example, stainless steel and titanium-based alloys have much higher Young's modulus (more than 100 GPa) than that of bone structure which is in the range of 10–30 GPa. This big difference of Young's modulus between the metallic implants and human bone can cause stress shielding effect on the peri-implant bones loss and even result in adsorption of adjacent bone tissues and cause prosthetic loosening. The other issue is that the radiopacity of metals limits the ability to examine the patient by X-ray computed tomography (CT) and magnetic resonance imaging (MRI) (Kurtz and Devine, 2007). As for

*Corresponding author.
E-mail address: H.Ou@nottingham.ac.uk (H. Ou).

http://dx.doi.org/10.1016/j.jmbbm.2016.07.027
1751-6161/

ceramics, there has been a great deal of attention devoted to advanced ceramic biomaterials in the past two decades. Bioactive ceramics exhibit favourable non-toxicity and corrosion-resistance, good biocompatibility and bioactivity. However, the mechanical properties of ceramics biomaterials, including low fracture toughness and ductility, high elastic modulus and brittleness, present a considerable challenge for meeting the demands of the load-bearing applications (Taskonak et al., 2006).

PEEK belongs to a class of materials known as two-phase semi-crystalline polymer, consisting of an amorphous phase and a crystalline phase. Following the confirmation of its biocompatibility two decades ago (Williams et al., 1987), poly (ether-ether-ketone) (PEEK) and its composites (Akay and Aslan, 1996; Meenan et al., 2000) such as carbon fibber reinforced (CFR) and hydroxyapatite (HA) filled and/or HA coated PEEK have attracted significant attention in using it for orthopaedic, trauma, and spinal implants in recent years (Kurtz and Devine, 2007). Compared with traditional metallic and ceramic implants, PEEK has several attractive properties. On the one hand, PEEK and its composites are radiolucent to X-rays. On the other hand, they have shown appropriate biocompatibility and comparable elastic modulus (3–4 GPa) to human bone structures, which is beneficial for the elimination of the extent of stress shielding that is often observed in titanium-based metallic implants. Therefore, PEEK and its composites are becoming more widely used as implant materials in orthopedics (https://www.victrex.com; Kurtz, 2012; Kayvon, 2013; Evans et al., 2015; Shimizu et al., 2016). Up to now, a number of experimental researches have been carried out to investigate the clinical performance of PEEK as a biomaterial for orthopedic, trauma, and spinal implants (Toth et al., 2006; Kim et al., 2009). Recently, Kurtz and Devine (2007) critically reviewed the biocompatibility and in vivo stability of PEEK, and gave an overview of the clinical applications of PEEK.

The assessment of the failure behavior of material plays a critical role in satisfying the fundamental needs for medical applications. Components can fail for a variety of reasons (Donald, 2013). Among these reasons, failure by fracture often originates from stress concentration under cyclic, static and impact loading. Therefore, the fracture properties of PEEK are of a great interest and importance leading to considerable attention in this field. In the past decade, investigations on the fracture properties of PEEK and its composite have been carried out (Chu and Schultz, 1989; Hamdan and Swallowe, 1996; Rae et al., 2007; Sobieraj et al., 2009, 2010; Berry et al., 1994; Mariconda et al., 2000; Garcia-Gonzlez, et al. 2015; Simsiriwong et al., 2015). A mechanism for defect-induced microcracks in the high stress concentration region near the crack tip due to the inclusion of impurities for PEEK was proposed by Chu and Schultz by using the impact tension test and scanning electron microscopy observation for the first time (Chu and Schultz, 1989). Rae et al. (2007) extensively investigated the mechanical properties of PEEK by using compressive and tensile experiments, and found that parabolic features and river markings are typical patterns for the fracture behavior of PEEK. And they pioneered to establish the qualitative relationship between the typical patterns and the crack tip, the growth direction of crack and the deformation temperature. Sobieraj et al. (2009, 2010) studied the fatigue behaviour and the fracture behaivor of pure PEEK by using circumferentially grooved round bar specimens. They thought that notching plays a key role in reducing the maximum true axial stress and maximum true axial strain, and they also determined the stress-life (S-N) behaviour of PEEK in the presence of stress concentration for the first time. But the research work by Rae et al. (2007) and Sobieraj et al. (2009, 2010) did not consider the effects of second phase impurities/inclusion on the initiation of fracture. Recently, Simsiriwong et al. (2015) analysed the effects of inclusions on fatigue life of PEEK, and established a microstructure sensitive fatigue model to predict the fatigue life of PEEK. In general, these studies gave detailed insights into the fracture properties of PEEK at both room and elevated temperatures. Based on these studies, several concrete suggestions have been offered on how to utilize PEEK in orthopaedic components (Rae et al., 2007; Sobieraj et al., 2009, 2010).

However, little attempt has been made to investigate the effect of stress concentration and inclusion on the fracture behavior of PEEK. As implant components tend to fail under static or repetitive loading due to stress concentration, an important implant design consideration is to achieve a long-term reliable performance under varied loading conditions. Although recent research has been reported in looking into orthopaedic fracture occurrence due to stress concentration along the rims of total disk replacements (Berry et al., 1994) and in noncruciate-sparing tibial components (Mariconda et al., 2000), there is a clear need for more detailed study of PEEK fracture in the presence of stress concentration. Furthermore no research has been conducted on the relationship between fracture patterns and stress triaxiality. Therefore, the objective of this study was to investigate the fracture behavior of PEEK under different stress states by using both notched as well as smooth specimens. Scanning electron microscopy (SEM) and finite element (FE) simulations were employed to characterise the fracture behaviors of PEEK. The primary chemical compositions of the inclusions were obtained by using an energy-dispersive X-ray spectroscopy (EDX) analysis.

2. Experiments

2.1. *Material description*

In this study, PEEK 450G extruded natural rod (Röchling Group, Germany) was used in testing. The diameter of the bar is 8mm. Mechanical and thermal properties of the material are given in Table 1. The crystallinity (fraction in mass) calculated from density is 38% (Bas et al., 1995).

Table 1 – Material properties of PEEK 450G.

Mechanical properties		Thermal properties	
Elastic modulus (GPa)	4.0	Thermal conductivity (W/mK)	0.25
Poisson's ratio	0.38	Specific heat (J/kg K)	2180
Density (kg/m3)	1310	Glass transition temperature (K)	425
Yield stress (MPa)	110	Melting temperature (K)	616

2.2. Design of specimens

In order to obtain different stress triaxialities, two groups of experiment were carried out. Group I includes axisymmetric notched specimens with the geometry and dimensions specified in Fig. 1a. The axisymmetric notched specimens were machined with notched radii of 0.5 mm, 1.0 mm, 2.0 mm and 4.0 mm. As shown in Fig. 1b, group II is composed by tensile tests of axisymmetric smooth specimens.

The initial stress triaxiality (σ^*) for axisymmetric rounded specimens can be obtained from the following equation (Bridgman, 1952):

$$\sigma^* = \frac{1}{3} + \ln\left(1 + \frac{r}{2R}\right) \quad (1)$$

where r is the radius in the minimum cross section area of the specimen and R is the notch radius. The axisymmetric specimens provide different initial stress triaxialities by means of changing the initial notch radius.

Assuming volume conservation, equivalent plastic strain can be obtained as a function of the cross section area or diameter as follows:

$$\varepsilon^p = 2\ln\left(\frac{d_0}{d}\right) = \ln\left(\frac{A_0}{A}\right) \quad (2)$$

where subscript "0" means initial value before deformation. In the uniaxial tensile test, the value of the axial strain is equal to the equivalent plastic strain. Thus equivalent plastic strain to fracture ($\varepsilon^p_{fracture}$) can be calculated by substituting d or A in Eq. (2) for $d_{fracture}$ and $A_{fracture}$, which are the minimum cross section diameter and area of the fracture specimen, respectively.

2.3. Testing methods

As shown in Fig. 2, the notched specimens were clamped between grips, and the tensile tests were carried out by using an INSTRON servo hydraulic universal testing machine. The tests were conducted at room temperature under a strain rate of 0.1 s^{-1}. The specimens were instrumented with a video gauge to

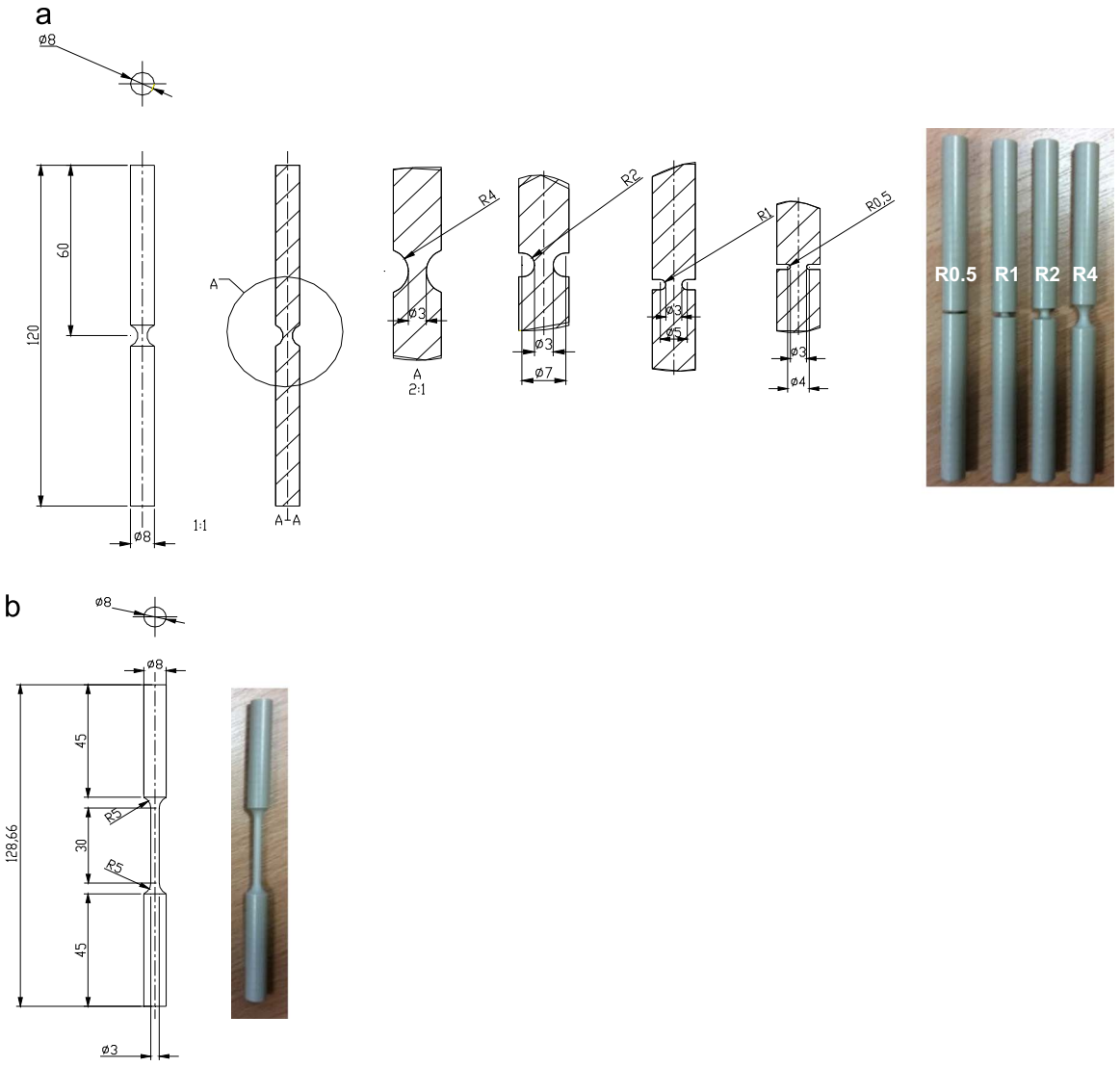

Fig. 1 – Geometry and dimensions of (a) axisymmetric notched specimens (R=0.5 mm, R=1.0 mm, R=2.0 mm and R=4.0 mm) and (b) smooth axisymmetric specimens.

measure the axial strain. In order to ensure the reproducibility, all the experiments were repeated twice.

After tensile tests, the fractured specimens were cut to a length of about 15 mm by an alloy wheel cutting machine. The sectioned specimens were polished down to 12 mm to make sure the bottom surface of specimen as flat as possible by using 240-grit and 400-grit SiC papers. Then the specimens were sticked onto a plate for coating to keep good electrical conductivity for SEM investigation. Finally, fracture patterns and inclusions were investigated by using a Philips (FEI) XL 30 SEM.

3. Results and discussion

3.1. *Load-displacement curves*

Fig. 3 contains four black and white images which show the evolution of the specimen with notched radius of 4 mm during the tensile test. It can be found that, when the specimens start necking (Fig. 3b), the circular notch shape is distorted. Significant necking took place in the notched specimen with propagation of the neck sometimes extending throughout the entire gauge length (Fig. 3c).

Load–displacement curves of notched specimens are given in Fig. 4. The load–displacement curves reveal that there is a dramatic decrease in the applied load once necking occurs, with the load remaining constant during propagation of the fully formed neck. At the onset of fracture, there is a slight dip in the load curve prior to rupture. As shown in Fig. 4, it can be found that the equivalent plastic strain to failure decreased remarkably with the decrease of notched radii. This suggests that the accumulation of plastic strain until the specimen's fracture was clearly geometry-dependent. It was noted that the amount of plastic strain necessary to fracture a notched specimen is decreased when a smaller notch radius is used.

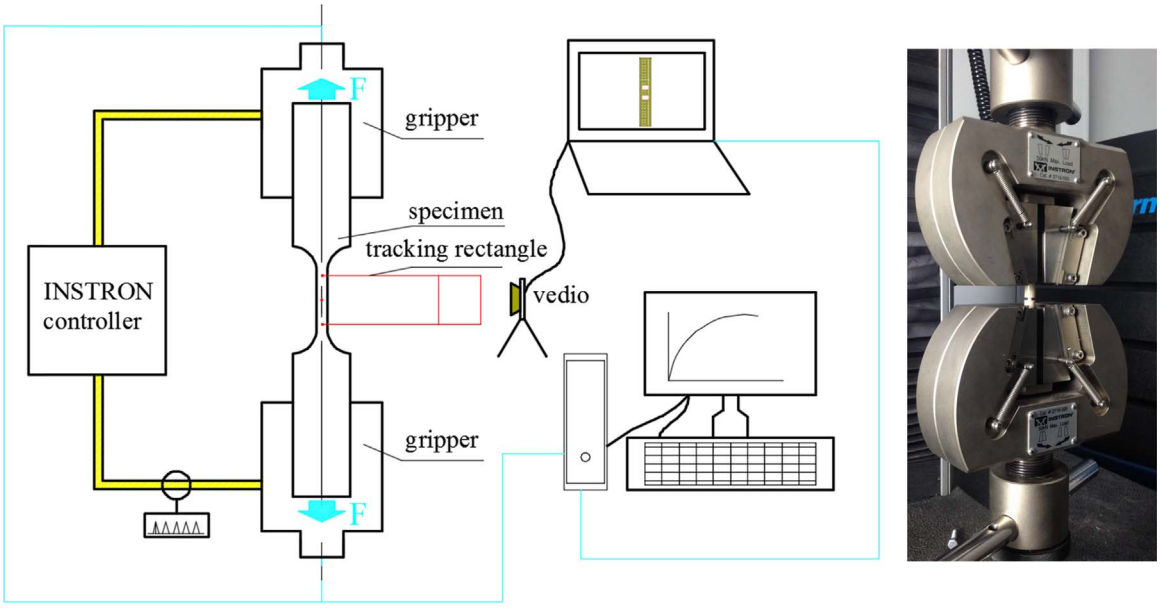

Fig. 2 – Schematic of the tensile test by using INSTRON. Machine.

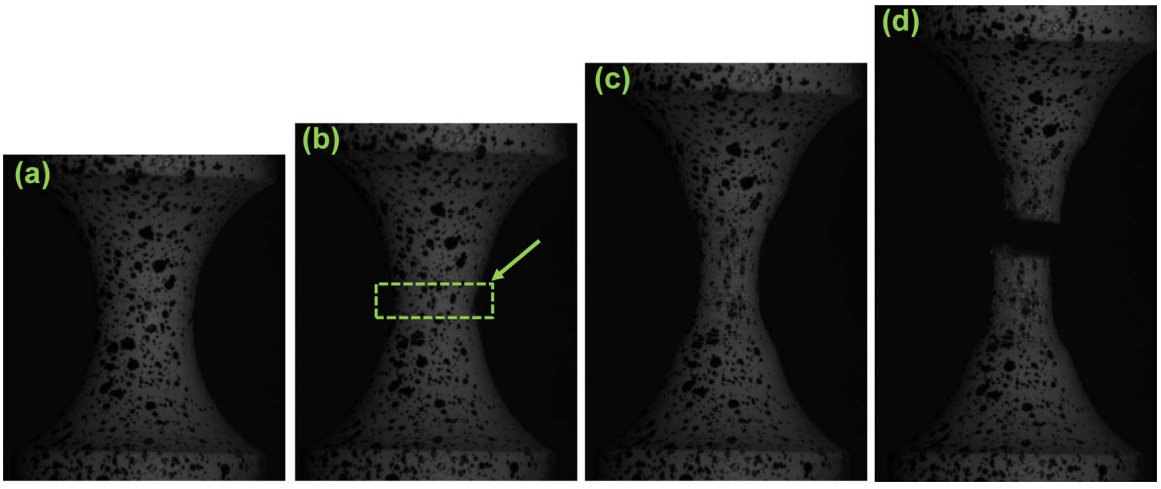

Fig. 3 – Stages of deformation in a notched specimen: (a) beginning of the testing, (b) onset of the necking, (c) propagation of the necking and (d) complete the fracture.

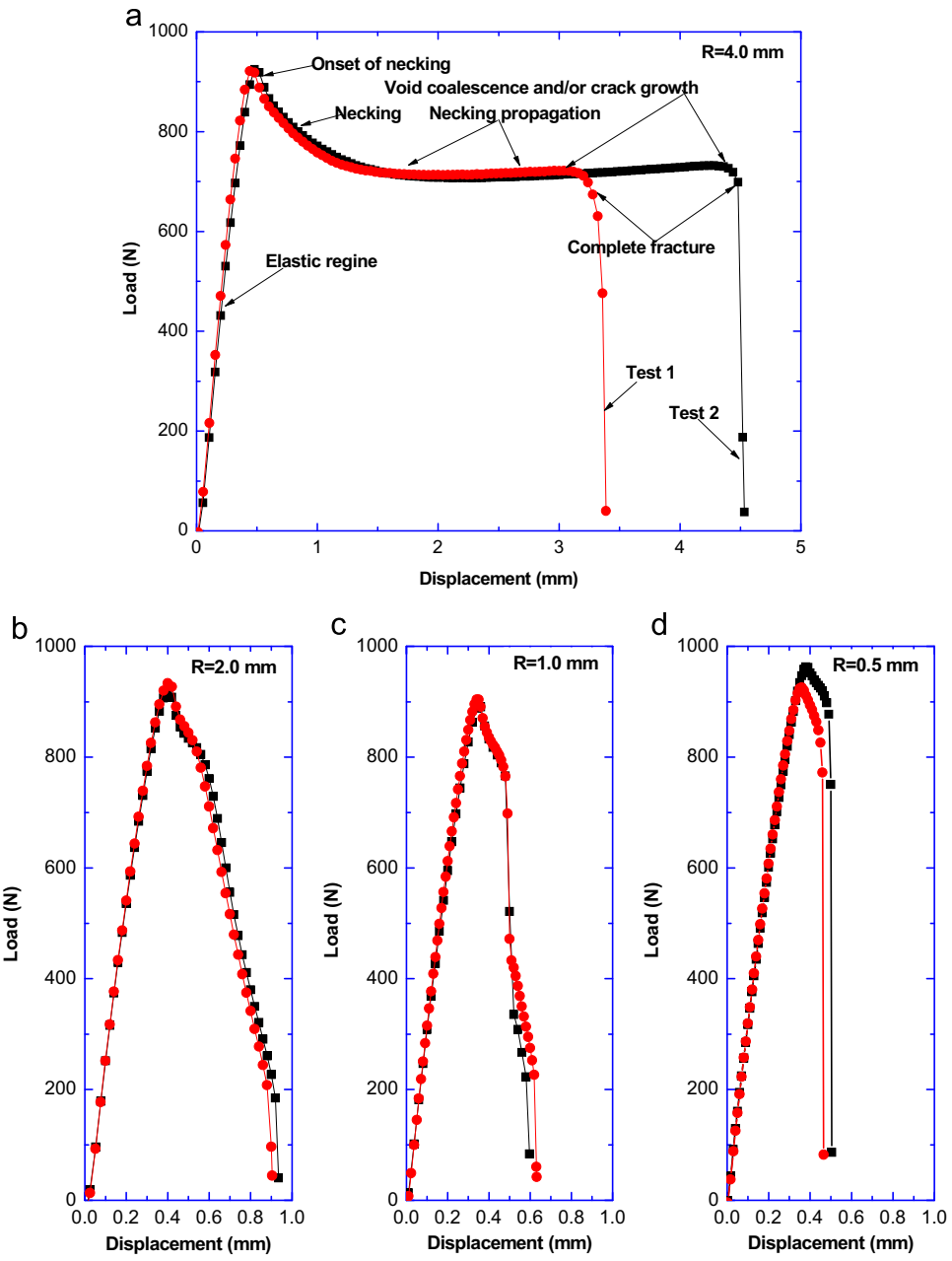

Fig. 4 – Load–displacement curves from notched axisymmetric specimens with radii of (a) 4.0 mm, (b) 2.0 mm, (c) 1.0 mm and (d) 0.5 mm.

Fig. 5 shows the fracture surfaces with different notched radii at relatively low magnification. The most interesting observation from the test is that the fracture patterns are distinctively repeatable for different notched specimens. This suggests that the stress triaxiality plays a key role in determining the fracture behavior of PEEK. In the following section more detailed discussion is provided on the fracture patterns under different stress triaxiality states.

3.2. *SEM observation of smooth specimen*

The fracture mechanisms of PEEK associated with different stress triaxialities were further evaluated by using SEM and EDX on the fracture morphologies of the failure specimens. For the smooth specimen group, as can be seen in Fig. 6, the fractures initiated in the interior of the specimen (Fig. 6a). The mechanism of fracture initiation depends primarily on void coalescence. Regardless of consecutive regions of fracture initiation (Fig. 6a), the main fracture pattern includes a region of crack growth (Fig. 6b), followed by a region of striations (Fig. 6c and d), with the striations becoming closer together as the distance from the initiation site increases. Finally, there is a transition region (Fig. 6e) to a fast fracture region (Fig. 6f). From Fig. 6, it is obvious that the entire fracture surface at low magnification looks very much like a circular shape, which suggests uniform propagation in all directions. These parabolic

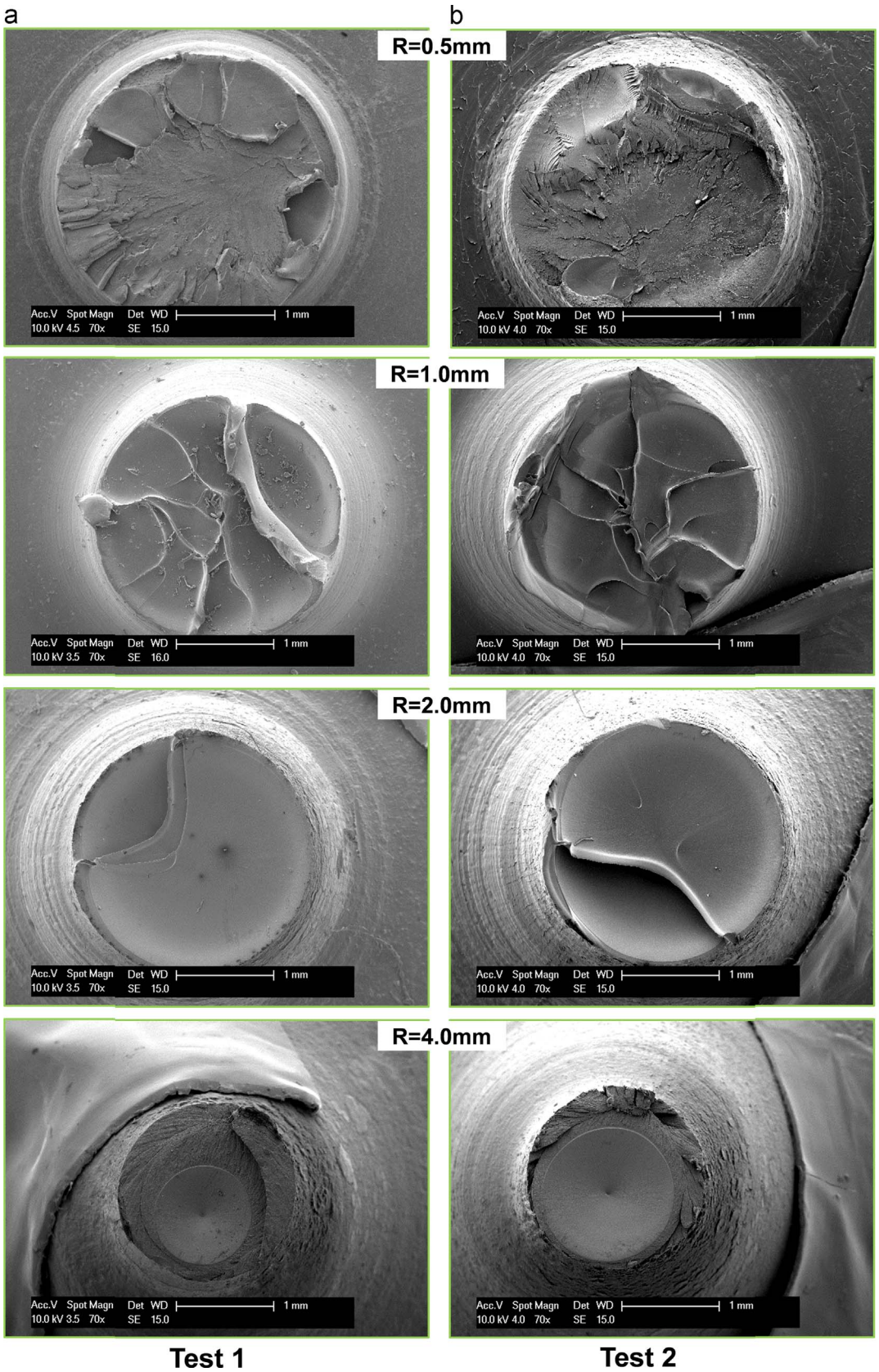

Fig. 5 – Representative macroscale fracture surfaces of PEEK notched specimens.

features have previously been observed in PEEK 450G in regions of high stress concentration, although it is not directly correlated to the crack-tip plastic zone (Chu and Schultz, 1989; Rae et al., 2007).

3.3. SEM observation of notched specimens

As shown in Fig. 7, the fracture micomechanism changed greatly with a notched radius of 0.5 mm. It is clear that void coalescence (Fig. 7-V) is ahead of the fast fracture region (Fig. 7f). It is worth noting that parabolic features were observed close to the edge of the fracture plane (Fig. 7a). As for parabolic features, the main fracture pattern includes critical crack initiation (Fig. 7b) and drawn finger-like morphology (Fig. 7c). Compared with the parabolic patterns obtained from smooth specimen, no fine striations zone was observed. Karger-Kocsis and Friedrich (1986) reported characteristic striations representative of plastic flow. It indicates that the deep notched specimens with a radius

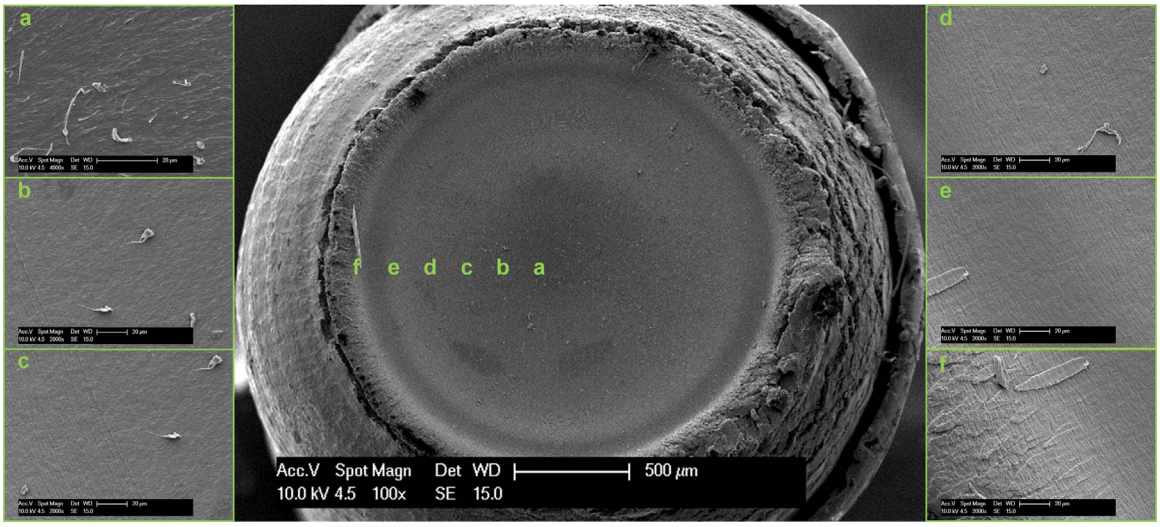

Fig. 6 – SEM fractograph of a smooth specimen. Zoomed in views of the labelled regions surrounding the main fractograph: a) critical flow/crack initiation, b) slow crack growth, c and d) striated regions, e) a transition region, f) fast fracture region.

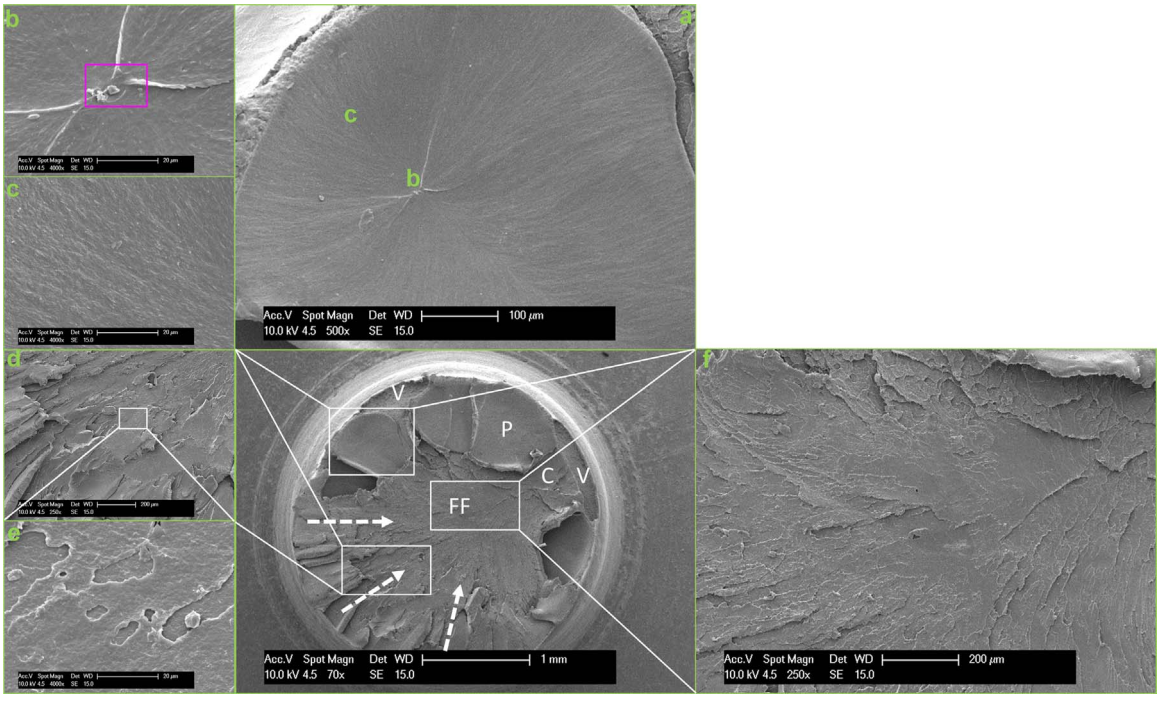

Fig. 7 – SEM fractograph of a notched specimen with a radius of 0.5mm. Zoomed in views of the labelled regions surrounding the main fractograph: a) large parabolic feature (P), b) critical crack initiation, c) drawn finger-like morphology, d and e) the patchwork morphology indicative of crazing, f) fast fracture region (FF). Regions of void coalescence (V), pathchwork morphology indicating fracture through crazes (C). (For interpretation of the references to color in this figure, the reader is referred to the web version of this article.)

of 0.5 mm undergo small plastic flow. Generally, the observed fracture patterns are consistent with other studies where, crack initiation took place due to the void coalescence. Accompanied with the crack proceeding inward, the regions of patchwork morphology appeared (Fig. 7d and e). As shown in this figure by using the dashed arrows, this process is also consistent with crack growth through crazes. It is clear that these patches became finer and more numerous in the direction of crack advance. Finally, in the central location of the notched specimen, there was a region of fast fracture (Fig. 7f).

The SEM images and EDX analysis of a notched sample with inclusion are shown in Fig. 8. A pink box in Fig. 7a denotes the area for the EDX analysis with an individual inclusion observed. The shape of the inclusion varies between rectangular-like and diamond-like with intermediate shapes in between. The size of the inclusion is about 1.5 μm. And the chemical composition of the inclusion is as following (wt%): 41.19% of oxygen, 21.26% of carbon, 22.95% of calcium and 14.59% of magnesium. It was also found that the surface area of a PEEK sample with no inclusion generally consists of 77.34% of carbon and 22.66% of oxygen by weight as reported in Fig. 8.

Fig. 9 shows the fracture plane under the notched radius of 1.0 mm. It is obvious that large parabolic features are a typical pattern (Fig. 9P). Many dispersed flakes can also be observed in the parabolic regions. From Fig. 9 (P-1 and P-2), it is worth noting that the parabolic shape becomes larger with increased number of dispersed flakes. Fig. 10 shows the SEM images and EDX analysis report of 1.0 mm notched specimen.

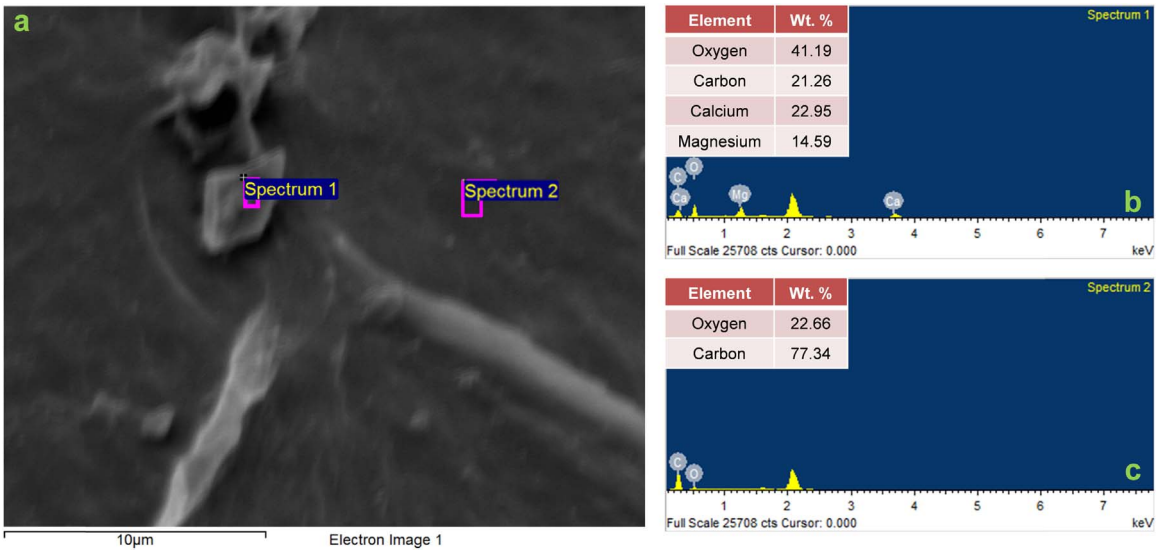

Fig. 8 – SEM image and EDX analysis: (a) SEM image of inclusion, EDX analysis showing (b) the chemical composition of the inclusion and (c) the matrix close to the inclusion zone.

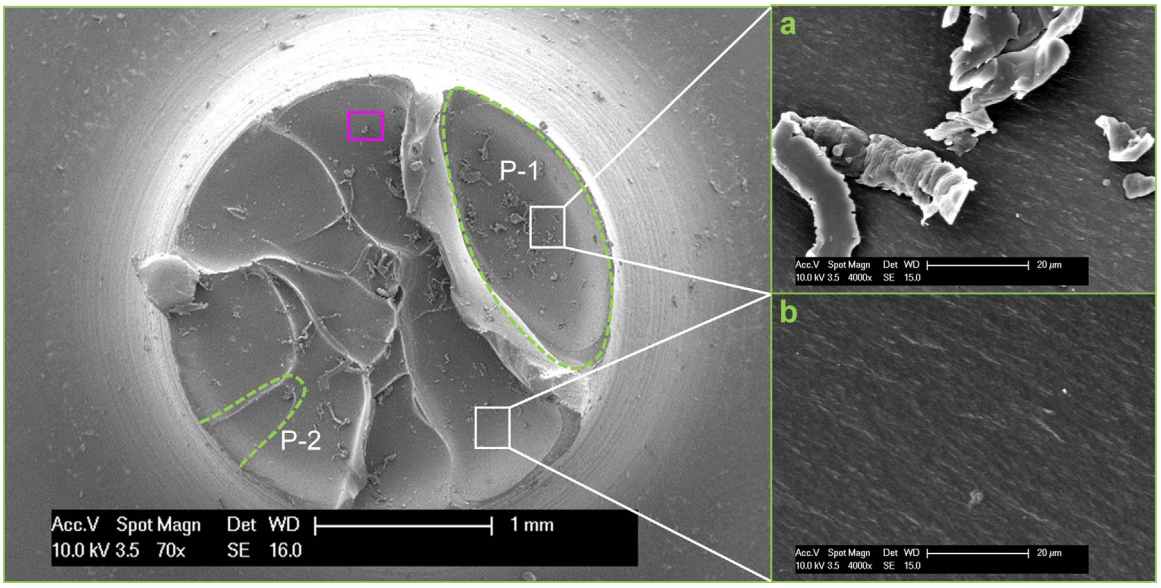

Fig. 9 – SEM fractograph of a notched specimen with a radius of 1.0 mm: (a) dispersed flakes in the parabolic region and (b) the drawn finger-like morphology. (For interpretation of the references to color in this figure, the reader is referred to the web version of this article.)

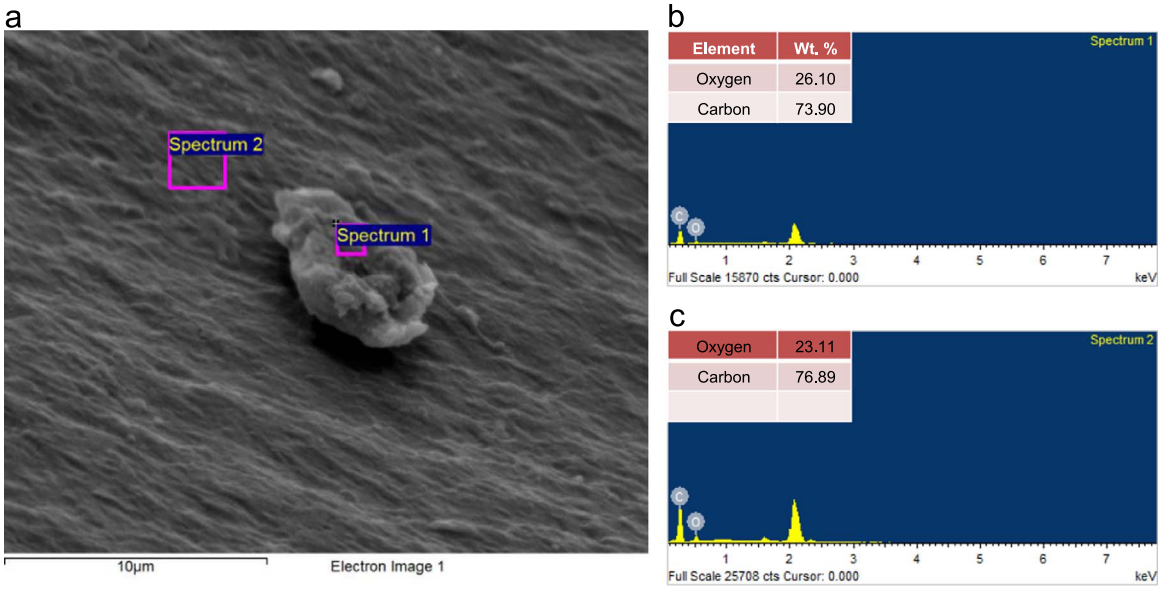

Fig. 10 – SEM image and EDX analysis: (a) SEM image of the flake, EDX analysis showing (b) chemical composition of the flake and (c) the matrix close to the flake zone.

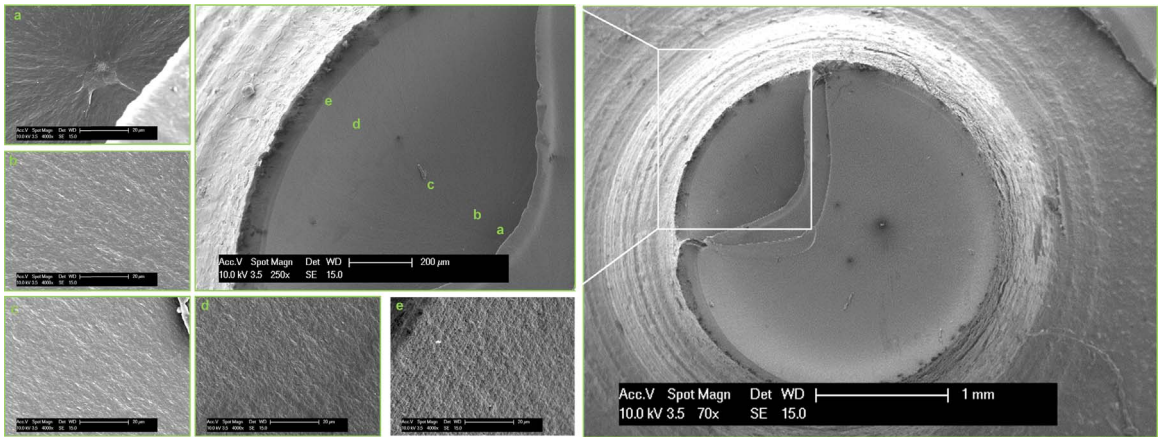

Fig. 11 – SEM fractograph of a notched specimen with a radius of 2.0 mm.

The pink box from Fig. 9 indicates the area of the EDX analysis performed. As shown in this figure, the chemical composition of the flake (73.90% of carbon and 26.10% of oxygen) was found to be comparable to that of matrix material (76.89% of carbon and 23.11% of oxygen). It is worth mentioning that these values are very much similar to the results obtained in Fig. 8c.

Figs. 11 and 12 show the fracture surface with notched radii of 2.0 mm and 4.0 mm, respectively. It is found that the fracture patterns are very similar to the findings of the smooth specimen as shown in Fig. 6. Fig. 13 also gives the SEM images and EDX analysis report of the notched sample with a radius of 4.0 mm. The pink box indicates the area of the EDX analysis performed (Fig. 12a). The chemical composition of the inclusion is as following (wt%): 11.92% of oxygen, 22.89% of carbon, 10.84% of chromium and 54.35% of ferrum. It is worth noting that these values are quite different from the results obtained in Fig. 8c. It means that different types of inclusions exist in the material.

3.4. *SEM observation in comparison with FEM simulation*

Fig. 14 shows the stress state of the notched specimens under tensile conditions. By using Eq. (1), the stress triaxiality with different notch radii can be also calculated as show in Fig. 14. It is clear that the value of stress triaxiality decreases greatly when the notched radius increases from 0.5 mm to 4.0 mm. Based on the above SEM investigations, it is clear that the stress triaxiality has a great effect on the fracture behavior of PEEK. To get an insight into the effect of stress concentration with different notched radii, numerical simulations of the tensile tests of axisymmetric notched specimens were carried out with ABAQUS/Explicit v6.13.

It is common knowledge that the change over from elastic state to plastic state is characterised by the yield strength of the

materials (Hill, 1998). And the fracture of ductile polymer has been confirmed to be the result of microscopic void nucleation, growth and coalescence (Brinson, 1970). Usually, ductile fracture of materials develops in three stages: during the first stage, when the matrix/particle interface stress has been elevated to the level where the particles either crack or de-bond from the matrix, the nucleation of micro-voids initiates at inclusions and second phase particles in matrix. In the second stage, it involves the dilatational and extensional growth of the micro-voids under the combined action of the applied triaxial stress condition and plastic strain. The final stage consists of the coalescence of micro-voids followed by the failure of the inter-void matrix, across a sheet of micro-voids, due to microscopic necking and localized plastic failure (Gdoutos, 2002; Sherry et al., 2008). It can be concluded that the von Mises/equivalent stress along the minimum cross section at the yield point plays a key role in determining the micro fracture behavior of the material. Therefore the von Mises/equivalent stress distribution

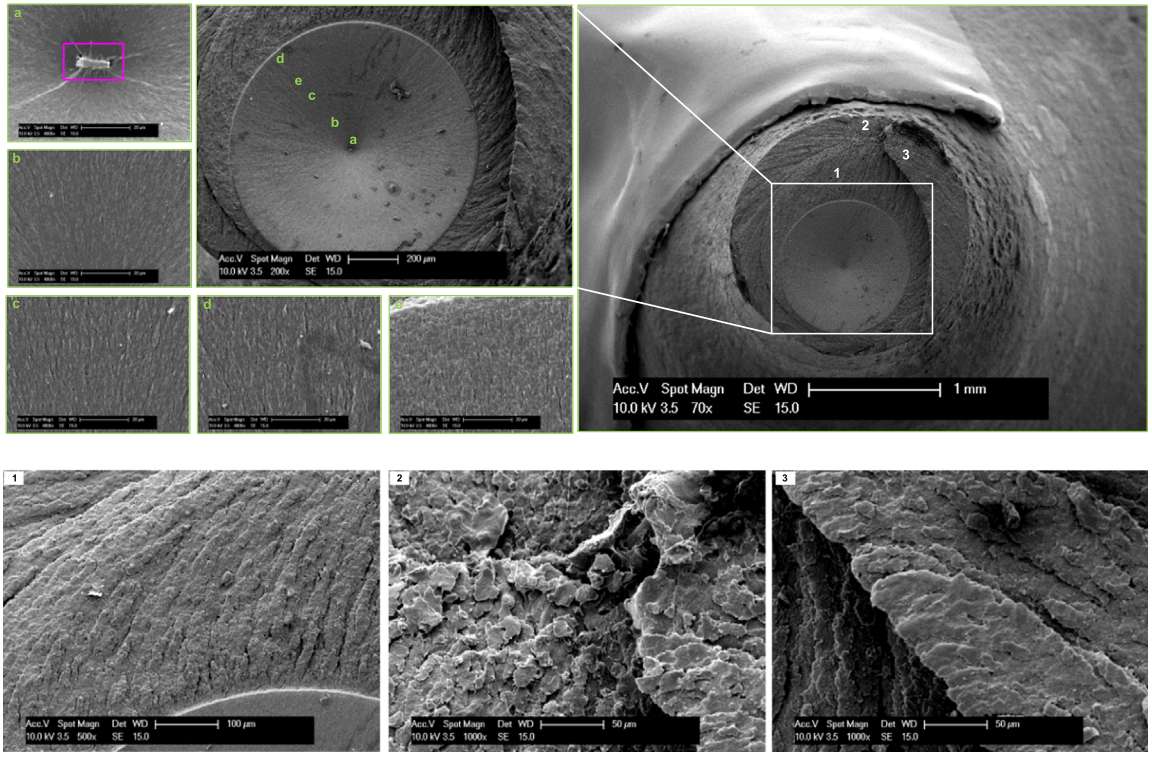

Fig. 12 – SEM fractograph of a notched specimen with a radius of 4.0 mm. (For interpretation of the references to color in this figure, the reader is referred to the web version of this article.)

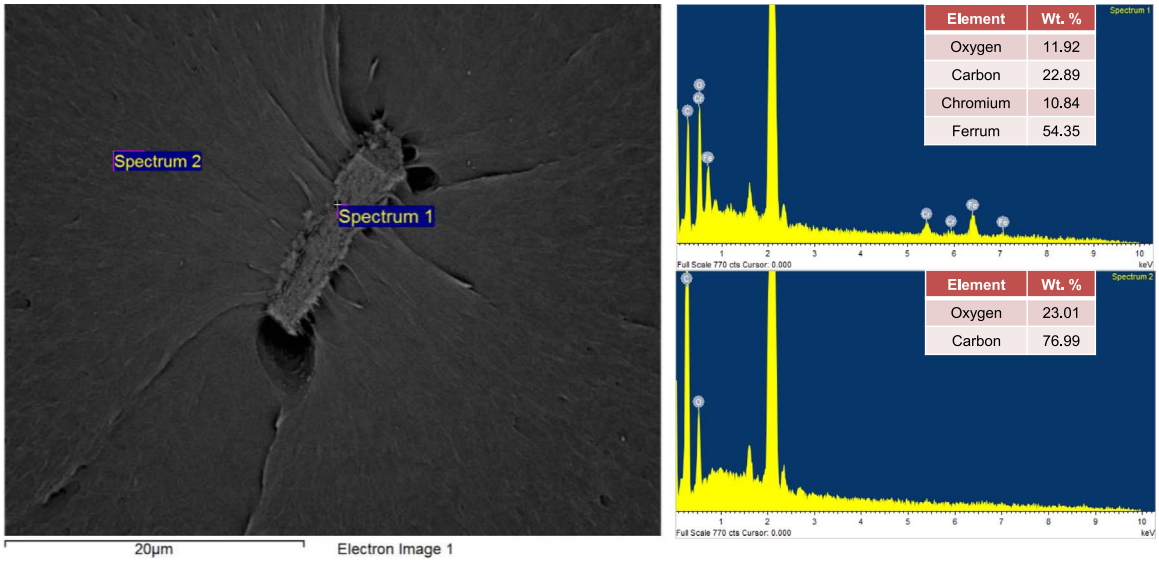

Fig. 13 – SEM image and EDX analysis: (a) SEM image of inclusion, EDX analysis showing (b) the chemical composition of the inclusion and (c) the matrix close to the inclusion zone.

of the minimum cross section of the notched specimens was firstly investigated by FE simulation. Fig. 15 shows the change of the von Mises/equivalent stress with deformation time steps at different nodal positions along the minimum cross section with notched radius of 0.5 mm. As can be seen in Fig. 15, it is easily found that the nodal positions of the minimum cross sections change from elastic to plastic deformation gradually. The surface of the notched region (N16 with Black Square in Fig. 15) becomes plastically deformed firstly and the centre of the specimen (N01 with purple vertical dash in Fig. 15) is the last to fall into the region of plastic deformation. It indicates that the nucleation of micro-void may firstly take place close to the surface of the notched specimen, and followed by the growth of the crack into the central region. As can be seen in Fig. 7, it is obvious that the crack-tip appears along the edge of the fracture surface. Fig. 16 gives the von Mises/equivalent stress distributions in the minimum cross section of notched specimens at yield point by FE simulation. At the same time, the difference of the Mises/Equivalent stress (σ_{eq}) and nominal stress (σ_{nom}) are illustrated. In this study, the nominal stress is calculated by using the following equation,

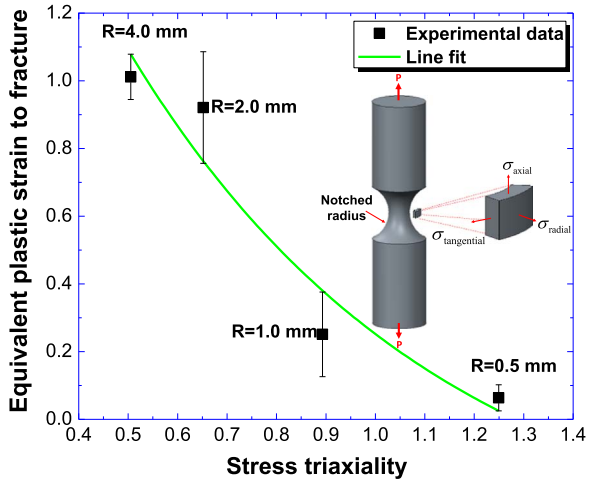

Fig. 14 – Equivalent plastic strain to fracture with the change of stress triaxiality.

$$\sigma_{nom} = \frac{1}{N}\sum_{i=1}^{N}\sigma_{eq}^{i} \quad (3)$$

As can be seen in Fig. 16, the difference between the von Mises/equivalent stress and nominal stress decreases greatly when the notched radius increases from 0.5 mm to 4.0 mm. The FE simulation results shown in Fig. 16, combined with previously SEM investigations given in Fig. 5, are used to determine the effect of stress state on fracture behavior/

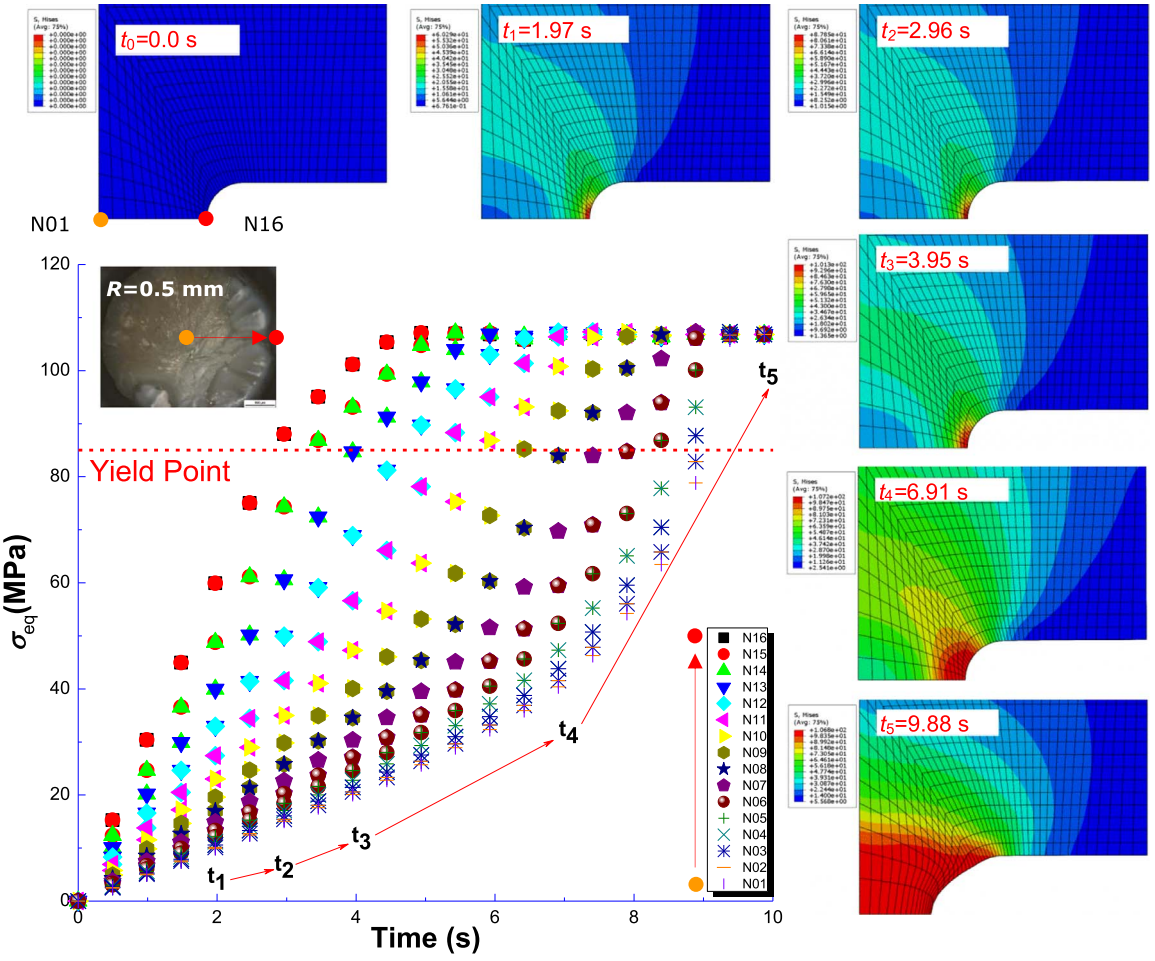

Fig. 15 – Mises stress with time for the notched specimen with a radius of 0.5 mm. N01 locates at the central of the notched sample, and N16 locates at the edge of the sample.

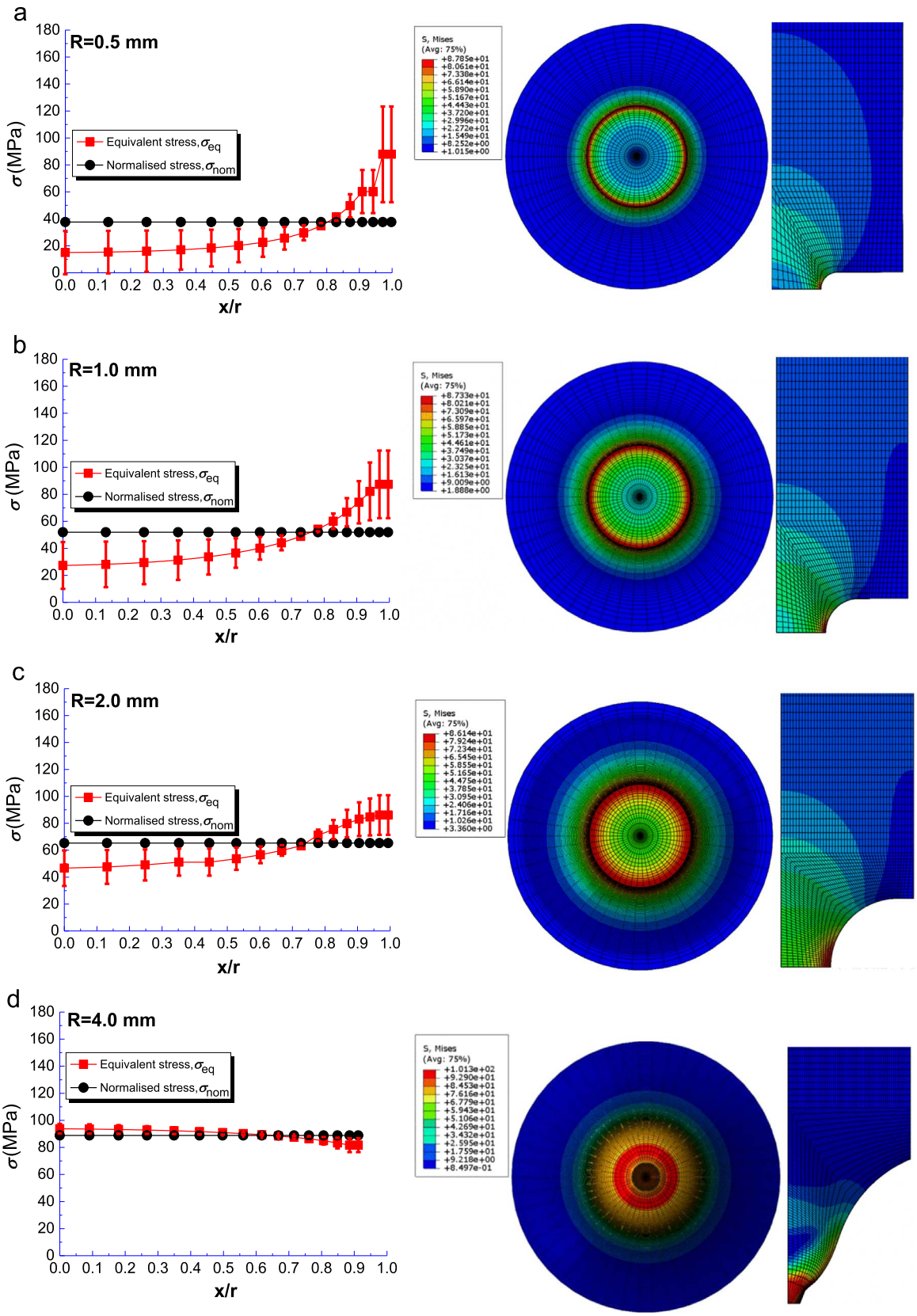

Fig. 16 – The difference between the Equivalent stress/Mises stress and Normalised stress at the yield point for notched radii of (a) 0.5 mm, (b) 1.0 mm, (c) 2.0 mm and (d) 4.0 mm. And the FM simulation results for the distribution of Mises stress.

fracture patterns of PEEK. Notched specimens with radii of 0.5 mm and 1.0 mm generate relative high stress triaxialities and high von Mises/equivalent stress gradient along the minimum cross section. This stress state has a clear effect to the nucleation, growth and coalescence of micro-voids from the edge of the specimen towards the centre. Notched specimens of radii of 2.0 mm and 4.0 mm cause relative low stress triaxialities and low von Mises/equivalent stress gradient along the minimum cross section. Hence it leads to more uniform nucleation, growth and coalescence of micro-voids as well as larger parabolic features as shown in Fig. 5.

Basic stress analysis calculations assume that the components are smooth and have a uniform section and no irregularities. In the design of implants by using PEEK they have at least minimal changes in section/shape. For example, PEEK transpedicular screw threads can change the stress distribution (Reinhold et al., 2007). Such discontinuities cause a local increase of stress, referred to as stress concentration which may cause the occurrence of fracture at early stage for the application of PEEK implants. Therefore, it is necessary to reduce stress concentration in PEEK implants design. The following methods can be used to reduce the stress concentration: i) using a number of small notches rather than a long one if a notch is unavoidable, ii) using stress-relieving grooves and iii) using narrow notches rather than wide notches if a projection is unavoidable (Pilkey and Pilkey, 2008). In recent years, with PEEK and related formulations being widely used into implant components (Evans et al., 2015; Steinberg et al., 2013), it is desirable for implant designers to think carefully about how this material behaves in terms of static and cyclic loading, particularly in the presence of stress concentrations. The findings from this study by the evaluation of macroscale and microscale of fractographs and FE results confirm the need for careful consideration in implant design by using PEEK.

Thermal aging has an apparent effect to crystallinity, crystallized structure and hence mechanical and tribological properties of PEEK material (Sınmazçelik and Yılmaz, 2007). Experimental results indicate that crystal growth and perfection process are in operation for short aging times at relative low temperatures. For higher aging temperature, initial aging promotes rapid crystal growth. Without consideration of aging effect, Therefore, it is intended to investigate the aging effect to the fracture characteristics of PEEK under different stress triaxialities.

4. Conclusions

Fracture behaviors of PEEK at different stress triaxialities were investigated by using tensile test of specimens with four different notched geometries and a smooth one. The typical fracture patterns and inclusions were analysed by using SEM and EDX. It is found that the stress triaxiality is the key parameter controlling the magnitude of the fracture strain for PEEK. Distinctive fracture patterns are observed (clearly shown in Fig. 5) at different notch conditions. It is proved that the failures initiated at randomly distributed weaker nucleation points due to inclusions, but the growth and coalescence of micro-voids are very much depends on the stress state. The ratio of σ_{eq} and σ_{nom} can be used as a key indicator to evaluate the discontinuity of the implant design for PEEK. It is important to carefully consider the location when utilizing PEEK as an orthopaedic component for notch riser.

Acknowledgments

This work was supported by the Engineering and Physical Sciences Research Council, United Kingdom (EP/K029592/1 and EP/L02084X/1), the Marie Curie International Incoming Fellowship (628055 and 913055), International Research Staff Exchange Scheme (IRSES, MatProFuture project, 318968) within the 7th European Community Framework Programme (FP7).

REFERENCES

Agarwal, R., González-García, C., Torstrick, B., Guldberga, R.E., Salmerón-Sánchez, M., García, A.J., 2015. Simple coating with fibronectin fragment enhances stainless steel screw osseointegration in healthy and osteoporotic rats. Biomaterials 63, 137–145.

Akay, M., Aslan, N., 1996. Numerical and experimental stress analysis of a polymeric composite hip prosthesis. J. Biomed. Mater. Res. 31, 167–182.

Bas, C., Grillet, A.C., Thimon, F., Albérola, N.D., 1995. Crystallization kinetics of poly (Aryl ether ether ketone): time-temperature-transformation and continuous-cooling-transformation diagrams. Eur. Polym. J. 31, 911–921.

Berry, D.J., Barnes, C.L., Scott, R.D., Cabanela, M.E., Poss, R., 1994. Catastrophic failure of the polyethylene liner of uncemented acetabular components. J. Bone Jt. Surg. 76, 575–578.

Bridgman, P.W., 1952. Studies in Large Flow and Fracture. McGraw-Hill, New York.

Brinson, H., 1970. The ductile fracture of polycarbonate. Exp. Mech. 10, 72–77.

Chu, J.-N., Schultz, J.M., 1989. The influence of microstructure on the failure behaviour of PEEK. J. Mater. Sci. 24, 4538–4544.

Diefenbeck, M., Mückley, T., Schrader, C., Schmidt, J., Zankovych, S., Bossert, J., Jandt, K.D., Faucon, M., Finger, U., 2011. The effect of plasma chemical oxidation of titanium alloy on bone-implant contact in rats. Biomaterials 32, 8041–8047.

Donald, J.W., 2013. Understanding How Components Fail, 3rd Edition ASM International, Materials Park, Ohio, USA.

Evans, N.T., Torstrick, F.B., Lee, C.S.D., Dupont, K.M., Safranski, D. L., Chang, W.A., Macedo, A.E., Lin, A.S.P., Boothby, J.M., Whittingslow, D.C., Carson, R.A., Guldberg, R.E., Gall, K., 2015. High-strength, surface-porous polyether-ether-ketone for load-bearing orthopedic implants. Acta Biomater. 13, 159–167.

Garcia-Gonzalez, D., Rusinek, A., Jankowiak, T., Arias, A., 2015. Mechanical impact behavior of polyether-ether-ketone (PEEK). Compos. Struct. 124, 88–89.

Gdoutos, E.E., 2002. Recent Advances in Experimental Mechanics. Springer, Netherlands.

Hamdan, S., Swallowe, G.M., 1996. The strain-rate and temperature dependence of the mechanical properties of polyether-ketone and polyetheretherketone. J. Mater. Sci. 31, 1415–1423.

Hill, R., 1998. The Mathematical Theory of Plasticity. Oxford University Press, Oxford.

Karger-Kocsis, J., Friedrich, k, 1986. Temperature and strain-rate effects on the fracture toughness of poly (ether ether ketone) and its short glass-fibre reinforced composite. Polymer 27, 1753–1760.

Kayvon, M., 2013. Handbook of Polymer Applications in Medicine and Medical Devices. William Andrew, Oxford, UK.
Kim, M.M., Boahene, K.D., Byrne, P.J., 2009. Use of customized polyetheretherketone (PEEK) implants in the reconstruction of complex maxillofacial defects. Arch. Facial Plast. Surg. 11, 53–57.
Kurtz, S.M., Devine, J.N., 2007. PEEK biomaterials in trauma, orthopaedic, and spinal implants. Biomaterials 28, 4845–4869.
Kurtz, S.M., 2012. PEEK Biomaterials Handbook. Elsevier, Amsterdam & London.
Mariconda, M., Lotti, G., Milano, C., 2000. Fracture of posterior-stabilized tibial insert in a genesis knee prosthesis. J. Arthroplast. 15, 529–530.
Meenan, B.J., McClorey, C., Akay, M., 2000. Thermal analysis studies of poly (etheretherketone) /hydroxyapatite biocomposite mixtures. J. Mater. Sci.: Mater. Med. 11, 481–489.
Pilkey, W.D., Pilkey, D.F., 2008. Peterson's Stress Concentration Factors. Wiley.
Poon, R.W.Y., Yeung, K.W.K., Liu, X.Y., Chu, P.K., Chung, C.Y., Lu, W.W., Cheung, K.M.C., Chan, D., 2005. Carbon plasma immersion ion implantation of nickel-titanium shape memory alloys. Biomaterials 26, 2265–2272.
Rae, P.J., Brown, E.N., Orler, E.B., 2007. The mechanical properties of poly (ether-ether-ketone) (PEEK) with emphasis on the large compressive strain response. Polymer 48, 598–615.
Reinhold, M., Magerl, F., Rieger, M., Blauth, M., 2007. Cervical pedicle screw placement: feasibility and accuracy of two new insertion techniques based on morphometric data. Eur. Spine J. 16, 47–56.
Sherry, A.H., Wilkes, M.A., Sharples, J.K., Budden, P.J., 2008. The assessment of residual stress effects on ductile tearing using continuum damage mechanics. J. Press. Vessel Technol. 130 (041212), 1–8.
Shimizu, T., Fujibayashi, S., Yamaguchi, S., Yamamoto, K., Otsuki, B., Takemoto, M., Tsukanaka, M., Kizuki, T., Matsushita, T., Kokubo, T., Matsuda, S., 2016. Bioactivity of sol–gel-derived TiO_2 coating on polyetheretherketone: in vitro and in vivo studies. Acta Biomater. 35, 305–317.
Simsiriwong, J., Shrestha, R., Shamsaei, N., Lugo, M., Moser, R.D., 2015. Effects of microstructural inclusions on fatigue life of polyether ether ketone (PEEK). J. Mech. Behav. Biomed. Mater. 51, 388–397.
Sınmazçelik, T., Yılmaz, T., 2007. Thermal aging effects on mechanical and tribological performance of PEEK and short fiber reinforced PEEK composites. Mater. Des. 28, 641–648.
Sobieraj, M.C., Kurtz, S.M., Rimnac, C.M., 2009. Notched sensitivity of PEEK in monotonic tension. Biomaterials 30, 6485–6494.
Sobieraj, M.C., Murphy, J.E., Brinkman, J.G., Kurtz, S.M., 2010. Notched fatigue behavior of PEEK. Biomaterials 31, 9156–9162.
Steinberg, E.L., Rath, E., Shlaifer, A., Chechik, O., Maman, E., Salai, M., 2013. Carbon fiber reinforced PEEK Optima – a composite material biomechanical properties and wear/debris characteristics of CF-PEEK composites for orthopaedic trauma implants. J. Mech. Behav. Biomed. Mater. 17, 221–228.
Taskonak, B., Mecholsky, Jr. J.J., Anusavice, K.J., 2006. Residual stresses in bilayer dental ceramics. Biomaterials 26, 3235–3241.
Toth, J.M., Wang, M., Estes, B.T., Scifert, J.L., Seim III, H.B., Turner, A.S., 2006. Polyetheretherketone as a biomaterial for spinal applications. Biomaterials 27, 324–334.
Williams, D.F., McNamara, A., Turner, R.M., 1987. Potential of polyetheretherketone (PEEK) and carbon-fibre-reinforced PEEK in medical applications. J. Mater. Sci. Lett. 6, 188–190.